Improving slope stability estimates by incorporating geophysical and remote sensing monitoring data into hydro-geomechanical modeling

Fiolleau Sylvain, Nicola Falco, Baptiste Dafflon, Sebastian Uhlemann

1. Lawrence Berkeley National Laboratory, Earth and Environmental Sciences Area, Berkeley, CA, USA

Correspondence to: S. Fiolleau, sfiolleau@lbl.gov

This manuscript has been submitted for publication in Geomorphology.

Abstract

Landslides are a major natural hazard, threatening communities and infrastructure worldwide. The mitigation of these hazards relies on the understanding of their causes and triggering processes, directly depending on soil properties, land use, and their variations over time. In this study, we propose a new approach combining geophysics and remote sensing with hydrological and geomechanical modeling to provide a robust estimate of the probability of failure of slopes in endangering the surrounding structures. Knowing that soil properties are site-dependent, it is crucial to analyze their sensitivity in estimating the probability of failure. Therefore, we performed a sensitivity analysis on the seven main parameters (density, friction angle, cohesion, soil thickness, slope, water recharge and saturated hydraulic conductivity) of the hydro-geomechanical model, which highlighted strong sensitivity to variations in soil thickness and cohesion. Based on those results, we used seismic noise measurements to assess soil thickness around our study site, which is a densely developed urban site. We highlighted that relatively thick soil layers (above 2 m) have up to 4 times higher probability of failure. Next, we used remote sensing data to assess vegetation cover. In fact, the presence of vegetation has a significant effect on soil cohesion, especially when the soil layer is relatively thin. The addition of vegetation cover showed an important reduction in the probability of failure when the soil thickness is less than 3 m.

Keywords: landslide risk, Probability of failure, Geophysics, Remote Sensing

1. Introduction

Landslides are a major natural hazard endangering communities and infrastructures. The assessment of risks generated by these hazards is critical considering the casualties and economic losses generated during the last decades (Froude and Petley, 2018). Haque et al.

(2019) shows that in 20 years (1995-2014) landslides caused a total of 163,658 deaths worldwide. According to the USGS, in the United States, landslides cause an estimate of more than $1 billion in damages and about 25 to 50 deaths each year. The assessment of these risks is all the more important as the current context of climate change leads to an increase in natural risks such as landslides (Coe, 2020; Lin et al., 2020; Patton et al., 2019).

Corominas et al. (2013) showed that the risk linked to the occurrence of a landslide depends on the hazard, the exposure, and the vulnerability. The landslide hazard is characterized by its susceptibility and its intensity, while landslide exposure is directly related to the elements at risks such as population, property, etc. This shows that urban areas with high probability of failure (PoF) have a very high landslide risk, and hence providing accurate estimates of the PoF is critical to assessing the risk (Cheung, 2021). The landslide susceptibility can be assessed through different approaches, depending on prior knowledge and the scale of the studied area. The three main approaches can be classified as heuristic, statistical or deterministic (Guzzetti et al., 1999; Regmi et al., 2014). The heuristic method, frequently used during the 70's and 80's (Aleotti and Chowdhury, 1999), involves geomorphological mapping of type and degree of the hazard based on expert knowledge. A major drawback of this method is the subjectivity in selecting data and factors governing slope stability. Statistical methods are a commonly used approach to evaluate landslide susceptibility in large or inaccessible areas and are based on multivariate and bivariate statistical techniques (Kalantar et al., 2020; Reichenbach et al., 2018), linking geological and geomorphological information with former landslide distributions. Among the most commonly used are linear regression (Akgun, 2012; T. Chen et al., 2016; Devkota et al., 2013; Park et al., 2013), artificial neural network (Gorsevski et al., 2016; Li et al., 2021; Nourani et al., 2014; Tien Bui et al., 2016; Tsangaratos and Benardos, 2014; Yilmaz, 2010a), support vector machine (Chen et al., 2016; Marjanović et al., 2011; Tien Bui et al., 2016; Yilmaz, 2010b), and random forest methods (Chen et al., 2017; Youssef et al., 2016). Deterministic methods are generally based on the calculation of the factor of safety (Regmi et al., 2014), which is the ratio of restraining to driving forces, and hence requires a numerical calculation of the forces acting onto a slope. Static or dynamic approaches can be used. For the static approach, the triggering factors are fixed contrary to the dynamic where those parameters are temporally variable. These methods require quantitative information such as hydrological information (soil saturation, permeability, hydraulic conductivity, etc.) and geotechnical information (soil thickness, cohesion, internal friction angle, density, etc.) (Jovančević et al., 2013; Montrasio et al., 2011; Palazzolo et al., 2021). The deterministic methods are considered more accurate than heuristic and statistical methods because physical processes are integrated and quantitative stability values are computed (Corominas et al., 2013). However, considering the large amount of a priori knowledge required, the application of those methods has been limited to local to regional scales (Cervi et al., 2010; Zizioli et al., 2013).

Deterministic approaches use physical models to calculate the stresses in the slope based on various governing equations and discretization. Hence, understanding the sensitivity of the input parameters on the results of a given model is crucial to understand the uncertainty of the results. Studies have shown that among all parameters integrated in slope stability analysis, the slope angle and soil thickness are the most sensitives (Choo et al., 2019; Min and Yoon, 2021; Segoni et al., 2012; van Westen et al., 2006). The sensitivity of other parameters can be more site-specific. For example, Choo et al. (2019) performed a sensitivity analysis on the slope stability calculations applied to Mt. Geohwa in South Korea and showed that while the slope angle and soil thickness strongly influence the factor of safety, also the friction angle had a strong impact on the slope stability estimation. The cohesion and density of the soil showed only minor impact. Given this variable sensitivity, which is a function of the chosen model, but also the characteristics of the study area, it is necessary to perform a sensitivity study to fully understand the uncertainties in the landslide hazard assessment for a certain area.

In addition to soil properties and slope loading, vegetation has also been recognized to play an important role on the stability of slopes (Band et al., 2012; Cohen and Schwarz, 2017; Hwang et al., 2015; Phillips et al., 2021; Sidle and Ochiai, 2006), but with varying effects. First, by adding weight to the slope, it can increase the load and reduce the stability, increasing the failure probability. However, in the case of a shallow landslide, this effect is largely compensated for by the increase in cohesion added by the root network and the reduction in moisture content (reduction in pore water pressure), thus increasing the factor of safety (Forbes and Broadhead, 2013). Among these factors, increasing cohesion has the largest influence on slope instability (Sidle and Bogaard, 2016; Sidle and Ochiai, 2006). To account for this, a simple approach is to directly add the cohesion induced by the presence of the root network to the soil cohesion (Emadi-Tafti et al., 2021; Ji et al., 2012; Kim et al., 2017; Mattia et al., 2005).

An important issue with the vegetation cover is that it is subjected to unpredictable variations over time (e.g. land management, wildfire). Wildfire constitute one of the main cause of vegetation destruction and plays a major role in landslide triggering (De Graff, 2018; Rengers et al., 2020). Numerous researches showed that root cohesion can be drastically reduced following fire lading to slopes more prone to failures (Gehring et al., 2019; Jackson and Roering, 2009; Lanini et al., 2009)

The spatial and temporal uncertainty of these input parameters is still one of the major challenges in predicting landslides (Anagnostopoulos et al., 2015; Sidle and Ochiai, 2006; van Westen et al., 2006). To consider this uncertainty, a probabilistic approach can be used (Hammond et al., 1992; Lee et al., 2020; Nilsen, 2000; Strauch et al., 2018). Strauch et al. (2018) developed a regional model of probabilistic slope failures and applied it to the North Cascades National Park Complex in the state of Washington, USA. They used a Monte Carlo simulation, facilitated by the python package *Landlab* (Hobley et al., 2017), allowing them to assess the uncertainty in model parameters and to highlight that soil thickness has a high influence on the landslide prediction. They also highlight the stabilizing effect of tall vegetation.

The aim of this study is to show the importance of including detailed spatial distributions of soil thickness and vegetation into slope stability estimates, as these spatially varying inputs strongly affect the landslide hazard assessment. To do so, we evaluated the PoF over an urban area using a probabilistic approach implemented in *Landlab*. First, we perform a sensitivity analysis of all model input parameters using a variance-based method. The soil thickness and the slope angle are shown to be the most sensitive parameters for the slope stability assessment. However, those parameters are also known to show high spatial variability which has to be included in the landslide hazard assessment. Strauch et al. (2018) overcame this issue by using a Monte Carlo approach, simulating the response of various soil thickness distributions. Vegetation also varies over time, with natural cycles of germination, growth and death. The duration of these varies with the nature of the plant. In addition, in urban areas, land management can amplify these changes in vegetation distribution over time, and hence affect the slope stability through changes in the root cohesion. To overcome these difficulties, we propose a new approach, combining geophysical and remote sensing data to account for the spatial variability of the most important input parameters in the PoF calculation. First, we estimate the soil thickness thanks to seismic ambient noise measurement and the computation of the H/V (Horizontal to Vertical) ratio. Then, we classify satellite images to retrieve the distribution of the vegetation cover over two periods encompassing a tree removal for wildfire hazard mitigation. By comparing the resulting PoF maps, we are able to highlight the influence of the model input parameters on the slope stability assessment. We show that by including detailed spatial estimates of soil thickness and vegetation distribution, we can provide improved estimates over time of the landslide hazard, which will aid in the urban landslide risk management.

2. Study site

The study site is located in the San Francisco Bay Area on the western flank of the northwest-trending Berkeley Hills (Figure 1). The seismically-active San Francisco Bay area includes a series of major northwest-trending active faults. The closest of these faults is the Hayward Fault, which lies near the base of the hills. The Hayward fault is among the fault systems with the highest probability of generating a large-magnitude earthquake within the next 30 years (WGCEP, 2008).

The site exhibits a significant landslide hazard due to its geologic and geomorphological history. The bedrock geology is complex in this part of the Berkeley Hills, comprising a variety of moderately to highly deformed sedimentary, volcanic, and metamorphic rock units. The oldest formation corresponds to the Great Valley Complex (Jurassic-Cretaceous, 159 – 99Ma) originally deposited in a marine environment, which is locally overlain by sedimentary and volcanic rocks of Tertiary age. The Orinda Formation (13.5 -10.5 Ma) is described as distinctly to indistinctly bedded siltstone, claystone, sandstone, and conglomerate. The conglomerates were deposited under alluvial fan conditions, while the sandstone, claystone and finer-grained conglomerates were deposited as flood plain and channel materials (Jones and Curtis, 1991). The Miocene Moraga Formation (10.2 – 9 Ma) is of volcanic origin consisting of andesite and basalt flows (Wahrhaftig and Sloan, 1989). During the late Miocene and early Pliocene (11.2 to 3.6 Ma), an extended period of compression occurred, resulting in folding, faulting, and uplift of the Berkeley Hills. These processes weakened the formations in place at that time (i.e., siltstone and claystone and highly fracture and weathered with a silty to fine gravelly matrix), which are subject to landsliding and erosion. These formations outcrop or are covered by a thin layer of colluvium or fill material, mainly composed of clay soils with moderate to high expansion potential. Near the base of the hills, Quaternary-age colluvium and landslide deposits, of up to 30 m thick, locally overlie bedrock and alluvial deposits.

The study site has a long history of landsliding with the presence of large paleolandslides (Figure 1), and numerous recent and active failure. A network of five GPS stations has been installed in 2012 and is monitoring three of those (Cohen-Waeber, 2018, Figure 1). One of these landslide areas (LRA4), which is impacting a bridge critical for emergency response of the Berkeley Hills, is also being monitored using various geophysical and environmental sensors since 2019 (Uhlemann et al., 2021). This landslide can be described as a slow moving clay rotational slide (Hungr et al., 2014), which takes place in the clayey deposit corresponding to paleolandslide deposits overlying the Orinda Formation (Kropp Alan and Associates, 2006), which are only a few meters thick.

The tall vegetation cover of the study area comprises mostly Eucalyptus Globulus, but also pines trees and occasional coast live oak.

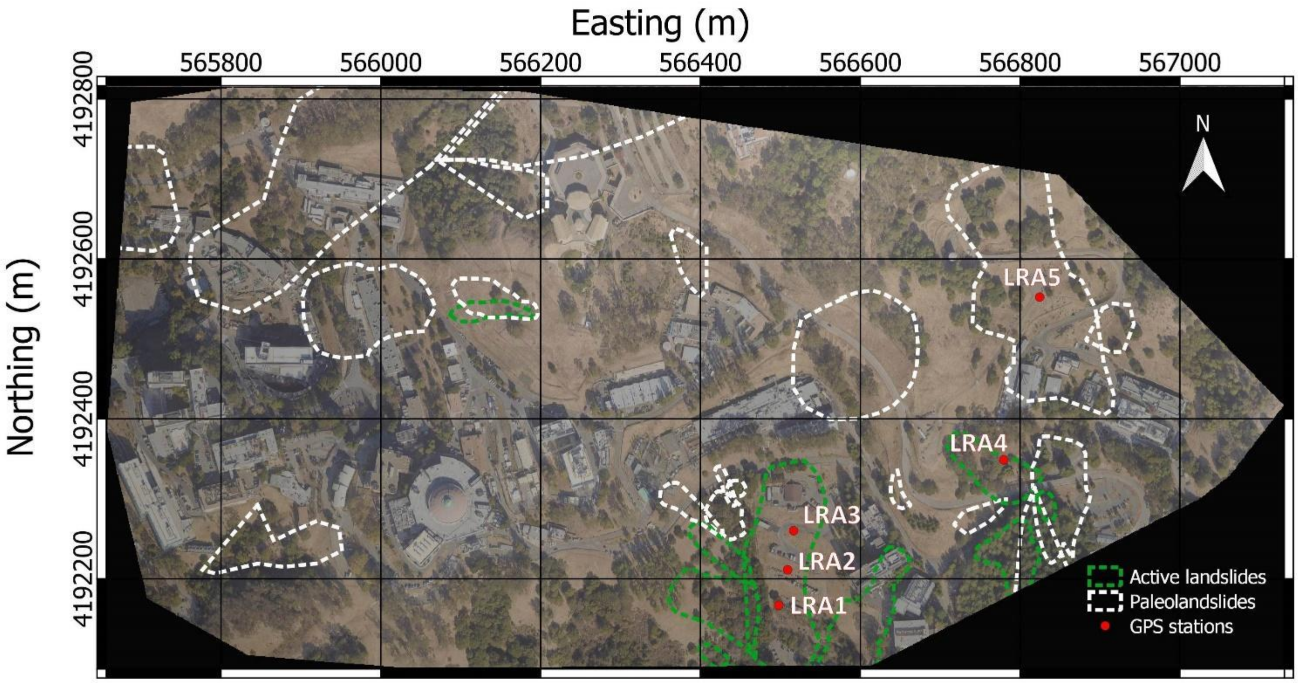

Figure 1 Study site map showing GPS stations (LRA1 to 5) locations and the footprint of paleolandslides and the active landslides.

3. Model and data inputs

3.1. Probability of failure (PoF)

Hazard assessment of the study area was performed by computing the PoF over a year. We used the LandslideProbability component of Landlab (Strauch et al., 2018) which used the common infinite slope stability model to compute the factor of safety (Eq. 1). This approach was preferred to others such as TRIGRS (Baum et al., 2008) to take into account the uncertainty introduced by the variability of some parameters (friction angle, water recharge) and also the promising results obtained with this method (Strauch et al., 2019).

$$FS = \frac{(C_s+C_r)/h_s\rho_s g}{sin\ \theta} + \frac{cos\ \theta\ tan\ \emptyset\ (1 - R_w\rho_w/\rho_s)}{sin\ \theta} \quad , \quad (1)$$

where C_s correspond to the soil cohesion (Pa), C_r to the root cohesion (Pa), $h_s$is the soil depth perpendicular to the slope (m), ρ_s and ρ_w correspond to the saturated bulk density and water density (kg.m^{-3}), respectively, g is the acceleration due to gravity (m.s^{-2}), θ is the slope angle (°) and Ø the soil internal friction angle (°). The relative wetness R_w is defined as:

$$R_w = \left(\frac{R\ a}{T\ sin\ sin\ \theta}, 1\right) \quad (2)$$

With R the uniform rate of recharge (md^{-1}) across the upslope specific contributing area a (m), and T the local soil transmissivity (m^{2}d^{-1}). Eq. 1 was solved using a Monte Carlo method with 1000 iterations, providing *a priori* distributions of the input parameters varying over one year.

Finally, the annual Probability of Failure, PoF at each model grid cell was calculated following

$$PoF = PoF(FS \leq 1) = \frac{n(FS \leq 1\ )}{N} \quad (3)$$

With n the number of iterations which met the failure criterion ($FS \leq 1$) and N the number of iterations.

Root cohesion calculation

As shown in the FoS calculation (eq1), the cohesion term is composed of the sum of soil and root cohesion. We calculated the root cohesion following the simple perpendicular root model (Waldron, 1977; Wu et al., 1979) which defines the total root induced cohesion (Cr) as:

$$Cr = Tr\ (sin\theta + cos\theta\ tan\emptyset)\left(\frac{Ar}{A}\right) \quad (4)$$

Tr is the average tensile strength of roots per unit area, $\frac{Ar}{A}$ (unit less) is the root area ratio (RAR), Ø is the angle of internal friction of the soil, and θ is the angle of deformed roots with respect to the shear surface. Based on an extensive sensitivity analysis, the value of $(sin\theta + cos\theta\ tan\emptyset)$ is often approximated to be 1.2 (Wu et al., 1979). However, it tends to overestimate the cohesion, so we applied a factor *k*" = 0.48, which is an empirical correction factor introduced by Preti (2006) to reduce the overestimated cohesion values, giving:

$$Cr = 0.48 * Tr\left(\frac{Ar}{A}\right) \qquad (5)$$

This corrected Cr has been shown to give results comparable to those obtained using fiber bundle models (FBMs) (Mao et al., 2014). Additionally, models such as energy-based FBM (Ji et al., 2020) might leads to more accurate and realistic Cr, but require more input parameters, such as the modulus of elasticity of roots, that we did not access in this study.

Next, we considered the three most represented tree species at the study site (pine trees, coast live oak and eucalyptus Globulus). We calculated the RAR at 10 cm depth intervals for Eucalyptus Globulus and Pinus Radiata species from Sudmeyer et al. (2004), and from Canadell et al. (1996) for coast live oak species. Root tensile strength data were extracted from Kuriakose and van Beek (2011) for Eucalyptus and pines species and from Norris (2005) for coast live oak species. This gave us a root cohesion values at 10 cm depth intervals to the maximum root depth for each species. For each depth, we computed the minimum, modal and maximum root cohesion.

Finally, for each pixel classified as tall vegetation, the minimum, modal and maximum root cohesion (C_r), at a depth corresponding to the soil thickness (calculated previously), was respectively added to the minimum, modal and maximum soil cohesion (C_s).

3.2 Model Inputs

The topographical data used for this study was derived from a digital elevation model with a 1 m resolution derived from a 2018-2019 USGS LiDAR dataset, obtained through the National

Oceanographic and Atmospheric Administration. The data set has a reported vertical accuracy of 0.087 m, with an average point density of the LiDAR data of 2.78 pts/m^2 (Quantum Spatial, 2019). Soil parameters were derived from previous geotechnical campaigns (Kropp Alan and Associates, 2006). The soil transmissivity, density and friction angle were set to 0.001 m^2/day, 1885 kg/m^3 and 24° respectively. Soil cohesion values were distributed with a minimum, maximum and modal cohesion of 5kPa, 15kPa and 7.75 kPa, respectively.

Soil Thickness

Soil thickness was mapped from previous geotechnical investigations and seismic ambient noise measurement. Previous active seismic campaigns showed that there is a high impedance contrast between the bedrock and the soil layer, revealing mean S-wave velocities of 250m/s ± 50m/s for the soil layer and about 750 m/s ± 90 for the bedrock (A3GEO, Inc., 2020). In such cases, using ambient noise recording, based on the horizontal to vertical spectral ratio technique (H/V technique), has been proven to be a robust and easy exploration tool for mapping the soil thickness (Guéguen et al., 2007; Le Roux et al., 2010). Measurements were performed with a three-component 4.5 Hz sensor at 31 locations (Figure 3, red points). Seismic noise was recorded during 3 hours at a sampling frequency of 200 Hz. Data were processed with the Sesarray package (Wathelet et al., 2004). Microtremor records were cut into 10 s time windows, for which Fourier spectra were computed and smoothed using the technique proposed by Konno and Ohmachi (1998). For each location, the H/V spectral ratios were computed for all time windows, and the mean H/V curve was determined with standard deviations For each point, the resonance frequency was extracted from the H/V peak exhibiting an amplitude larger than 3 (SESAME, 2004). From this resonance frequency (F_0, Hz), we calculated the soil depth (h, m) using the mean S-wave velocity (Vs, 250 m/s) following: $h=Vs/4F_0$ (Kramer, 1996).

Vegetation classification

Vegetation is an important agent in stabilizing steep slopes notably by increasing the soil cohesion for shallow landslides (Phillips et al., 2021). In some hard-to-reach areas, it may be difficult to assess the distribution of vegetation cover. Also, vegetation cover changes over time due to land management practices, as in our case for fire management, or wildfire (Rengers et al., 2020). Considering those frequent changes, we chose to use satellite image classification to extract vegetation cover in order to overcome those issues in a reproducibility sake.

The PoF calculation proposed by *Landlab* corresponds to the average PoF over a year. In order to extract the vegetation cover over two different periods before and after tree removal, an image classification was performed from four Planet images. Those images were acquired on October 26, 2020 and January 9, 2021 for the first period and on April 18 and June 29, 2021 for the second. Each image was composed of 4 bands (red, green, blue, and near infrared) with a resolution of 3 meters per pixel. Due to the relatively small size of the study area, the selection of training and testing samples and the classification were performed on 1647x1670 pixel images (4941x5010 m) including the study area. In a sake of future automatization of the process, same samples were used for both periods. Then, tiles were merged by period into a final raster composed of the 8 bands (2 acquisitions of 4 bands for each period) for classification using QGIS (2020).

The objective was to classify the image into 4 distinct classes: Tall vegetation corresponding to the tree coverage, low vegetation corresponding to shrubs, bare soil corresponding to grass or bare soil depending on the season, and others corresponding mainly to built environment.

A supervised classification was conducted using the sklearn python toolbox (Pedregosa et al., 2011). 100 points samples were selected for each class. These samples were split into 80 for training and 20 for testing. We tested two of the most widely used supervised algorithms, RF (Erinjery et al., 2018; Liu et al., 2018) and SVM (Falco et al., 2021, 2020; Mountrakis et al., 2011).

For the RF, hyper parameters including the maximum depth of the tree and the number of trees in the forest (n_estimators), were tuned by cross-validation in a search space with the following settings: max_depth = {1,2,…,20} and n_estimators= {1, 2, …, 300}. The cross-validation determines the best parameters for high classification accuracy to be a maximum depth of 12 and 9 associated respectively with a number of trees of 21 and 40 for the first and second period respectively. For the SVM, hyper parameters including the kernel (k), the regularization parameter (*C*), and the gamma parameter (γ), were tuned by cross-validation in a search space with the following settings: k= {'rbf', 'polynomial'}, C= {0.01, 0.1, …, 10000} and γ= {1×10^{-9}, 1×10^{-8}, 1×10^{-7}, …, 1000}. The regularization parameter defines the tolerance of the model to allow for misclassification of data points. The gamma parameter defines how far the influence of a single training example reaches. The cross-validation determines the best parameters for high classification accuracy to be a radial basis function (RBF) kernel with C = 100, γ = 1×10^{-7} and C = 10, γ = 1×10^{-6} respectively for the first and second period.

4. Results

4.1. Sensitivity analysis

Slope angle, soil thickness, and root cohesion have a strong impact on the calculation of the PoF. To estimate their importance compared to the other model input parameters, a sensitivity study was performed by calculating the Sobol indices using UQLab (Marelli and Sudret, 2014). The Sobol method, also called Analysis of Variance (ANOVA), described the total variance of the model in terms of the sum of the variances of the inputs (Sobol′, 2001). This approach allows to determine the influence on the model, of each input individually, excluding the interaction effect with other parameters, considering the first order indices. Figure 2 shows the first-order Sobol indices for each parameter and its calculated confidence interval for the 0:025 and 0:975 quantiles.

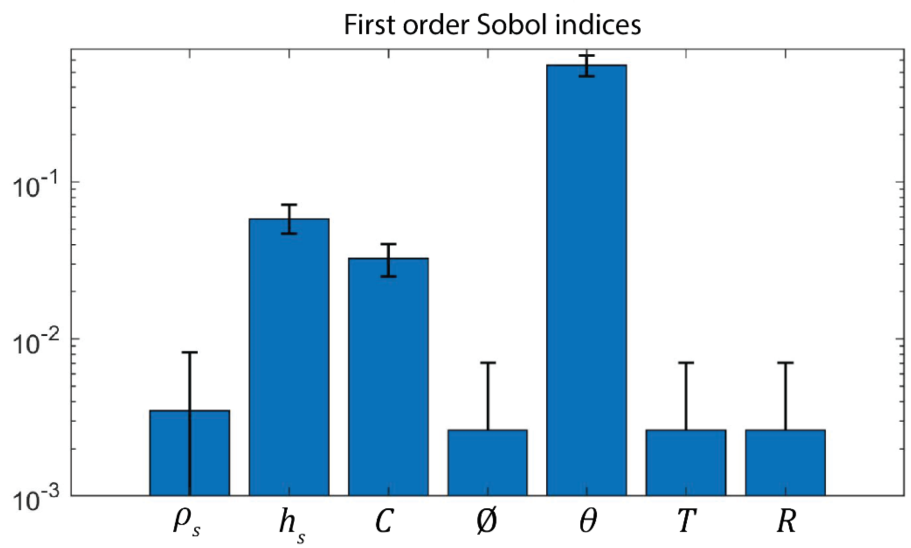

Figure 2. First Sobol indices of the 7 parameters (soil density ρ_S, Soil thickness h_S, Cohesion C, friction angle $\emptyset$, slope angle θ, transmissivity T and water recharge (amount and shape) R) used to calculate the factor of safety and its confidence interval.

The results show that soil density, friction angle, transmissivity, and water recharge have at least one order of magnitude less influence on the FoS than thickness, cohesion, and slope angle. This confirms that slope angle, soil thickness and the soil cohesion are the most critical parameters when evaluating the PoF using this probabilistic approach.

4.2. Soil Thickness variations

We mapped the soil thickness from geotechnical and H/V measurements (42 boreholes, 31 ambient noise recordings, Figure 3) using an inverse-distance-weighted (IDW) interpolation. Figure 3b shows two H/V analyses for a deep and a shallow bedrock. HV-1 shows a peak with an amplitude of 3.5 at 4 Hz, which leads to 15.6 m bedrock depth estimate. HV-2 shows a peak with an amplitude of about 7 at 35 Hz, estimating the bedrock to be at 1.8 m depth.

The uncertainty of the thickness map is related to bedrock depths values (Boreholes and H/V), the points density and the interpolation. For the bedrock depths values, the uncertainty is jus of few centimeters for boreholes and for HV it is directly related to the uncertainty on Vs, which ranges from 200 to 300m/s in our study case. This leads to an uncertainty of few cm for very thin soils until 3 m for the thickest areas (18 m) and ±0.65 m for the average thickness (3.25 m).

The soil layer is relatively thin over the study area showing an average thickness of 3.25 m, with a maximum of about 16 m in the eastern part of the study area and a minimum of 0 m corresponding to the location of bedrock outcrops. The eastern part has the thickest area associated with less excavations due the presence of fewer buildings. Figure 3c shows that the mean thickness is close to be constant around 3.25 m for all slope angles, except for flat surfaces where the mean thickness decreases to 2 m. However, the standard deviation shows larger values, highlighting the presence of greater soil thickness, for slopes ranging from 10° to 25°.

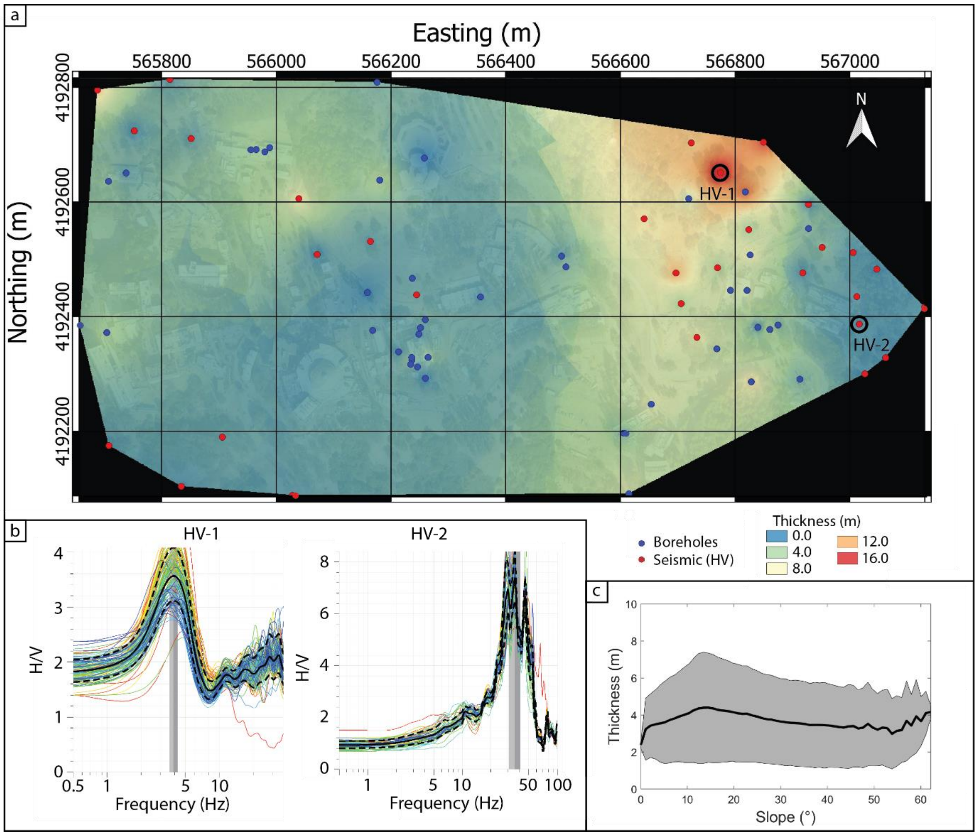

Figure 3 a) Soil thickness map interpolation from geotechnical (boreholes, blue points) and seismic data (HV measurements, red points). Google satellite background map. b) Examples of H/V curves in the thickest part of the soil (HV-1) and in a thin soil layer (HV-2). c) Mean thickness distribution and its standard deviation in function of slope angle.

4.3. Vegetation variation

In order to estimate the root cohesion, we first classified Planet images to find the vegetation cover in a reproducible way. Then, we added the additional cohesion to the PoF calculation based on this vegetation cover.

The RF classification classified the 5x5km area with an overall accuracy of 86% and 89.25% respectively for the first and second period, while SVM algorithm did classified it with an overall accuracy of 93.6% and 91.4% respectively for the same both periods. Considering those results, the SVM classification was used to extract the tall vegetation of the study area.

Figure 4 shows the result of the classification of the vegetation cover for the second period over the study area. Globally, all trees are classified as tall vegetation except for rare isolated trees which seem misclassified as bare soil. Our method for accounting for root cohesion only considers areas covered by tall vegetation as it is the only type of vegetation to have a root network able to stabilize soil thicker than 1 m. This type of vegetation represents about one third of the study area (Figure 6).

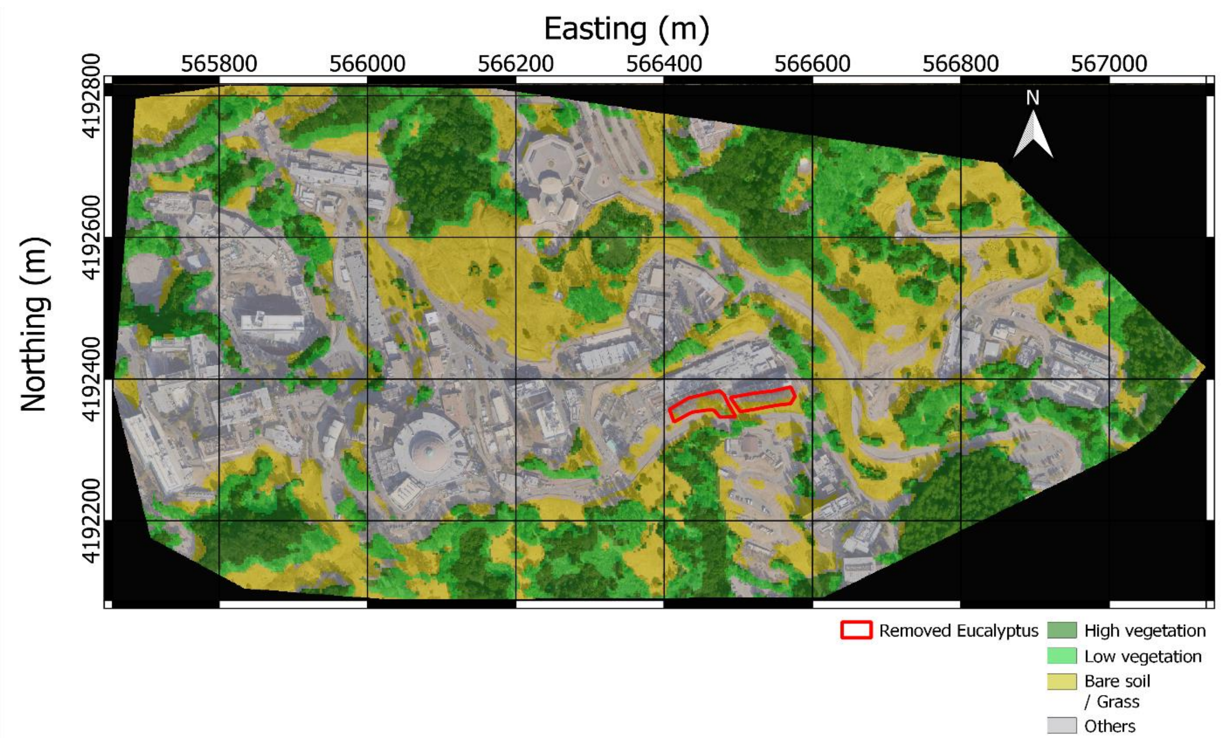

Figure 4 Result of SVM classification of the second period (April-June 2021): tall vegetation, low vegetation, bare soil and others over the study area.

4.4. PoFs

The influence in integrating soil thickness and root cohesion spatial variability in the PoF calculation is assessed through estimating the PoF in three different ways, (1) accounting only for slope angle (PoF_S), (2) including soil thickness (PoF_ST) and (3) including root cohesion (PoF_STV) based on the vegetation cover classification of the second period (April-June 2021).

The PoF of the study area was first evaluated considering only the slope angle (PoF_S, Figure 5a). To do so, the soil thickness was set to a constant 3.25 m (corresponding to the mean soil thickness over the study area), while no change in soil cohesion due to the vegetation was considered, and the other parameters were set as described in section 2. Figure 5b shows the distribution of slopes over the study area, highlighting numerous slopes greater than 40°, and up to 60° for some localized areas. The slope distribution and the PoF map are correlated, showing high probability (red areas) for slopes above 40°. The mean PoF_S over the whole study area is 0.26. Considering its spatial distribution, Figure 5a shows a high PoF on unbuilt areas, while flat areas (covered with building) show a negligible PoF.

Including the soil thickness in the PoF calculation, we can consider 2D variations of both the slope angle and soil thickness (PoF_ST, Figure 5c). The mean PoF_ST is 0.22. Figure 5c shows that the high PoFs (close to 1) are located in areas of thick soil cover (above 4 m). The difference between PoF_ST and PoF (Figure 5d) shows values increasing by up to 0.75 and values decreasing by as much as -1. The change in the PoF was calculated from the average soil thickness of 3.25 m corresponding to the boundary between the positive and negative impact of soil thickness variation (gray, Figure 5d). We observed a decrease for all areas exhibiting soil thickness below 3.25 m. Particularly in the central, eastern and southern part of the study area, the PoF_ST decreases from 1 to 0 due to a soil thickness below 1 m. On the contrary, PoF_ST increases for areas with soils thicker than average soil layer, particularly in the northeastern part of the study area.

Figure 5e shows the probability of failure taking into account variable root cohesion (PoF_STV). Overall, the mean PoF_STV over the whole study area decreased to 0.19. The PoF is distributed with high values in areas with greater soil thickness, and lower values in the south-western part of the study site (Figure 5e).

Looking closer at the difference between the two probability maps (PoF_STV-PoF_ST, Figure 5f), it appears that the probability decreases by up to -0.9 in places that are characterized by tall vegetation and thin soil cover, corresponding mostly to the south-western part.

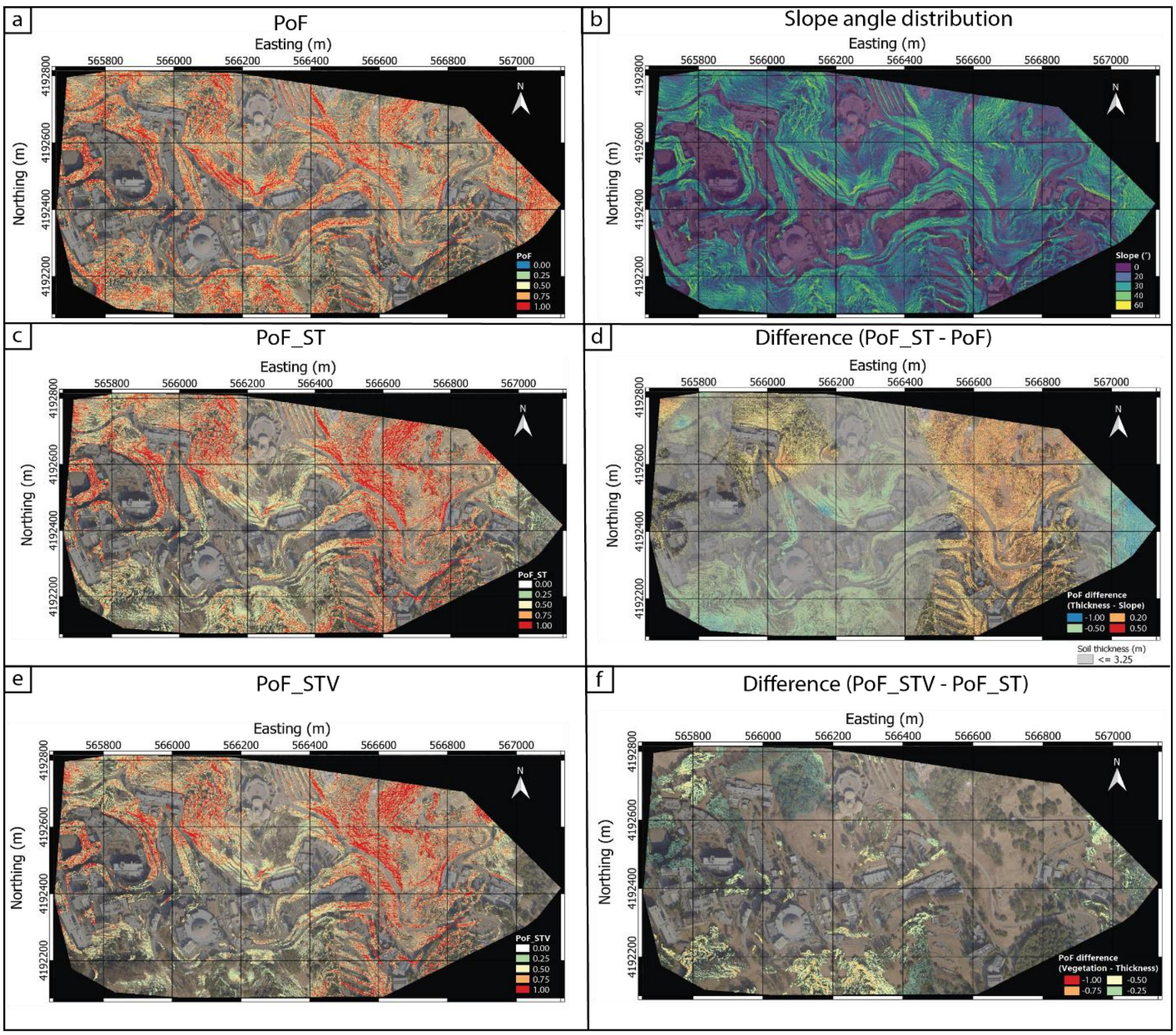

Figure 5 a) PoF map considering only slope variations (PoF_S). b) Slope distribution c) PoF map considering slope and soil thickness variations (PoF_ST). d) PoF_ST - PoF. e) PoF map considering slope, soil thickness and vegetation cover variations (PoF_STV). f) PoF_STV – PoF_ST.

Figure 6a shows the mean PoFs (PoF_S, PoF_ST and PoF_STV) and associated standard deviations as function of slope angle. The PoF_S is zero for slope angles below 18° (Figure 6a, black). Then, it increases linearly until reaching 1 for slopes above 42°. Areas with a high PoF (0.8 and above) are distributed across the entire study site (Figure 5a) and correspond to areas with slope angles greater than 35° (Figure 6a). Looking at the mean PoFs, considering variations of soil thickness and root cohesion tends to decrease significantly the probability for slopes between 25 and 60° (Figure 6a). We observed a slight increase of the mean PoF_ST and PoF_STV for slopes between 15 and 21° associated with a large variation of thicknesses due to the presence of higher soil thickness (Figure 3c). The PoF_ST shows a continuous increase from slopes of 20° until reaching high values (PoF > 0.9) for slopes ranging from 45° to 55°. Then, as for the PoF (black), PoF_ST is equal to 1 for slopes of 60° and greater. PoF_STV shows only a continuous increase, with smaller probabilities than PoF_ST, until reaching its higher value for slopes of 60° (Figure 6a).

Figure 6b and c shows the mean PoF_ST and mean PoF_STV, respectively, calculated from the PoFs maps (Figure 5c and e) as function of soil thickness and slope angle. Considering slope angle and soil thickness, PoF_ST and PoF_STV have similar pattern with high PoF for slopes above 30° and soil thickness above 5 m (figure 6b and c). PoF_ST and PoF_STV equal zero for slopes below 15° and thickness below 50 cm (Figure 6b and c). Thereafter, PoF_ST increase continuously until they reach high values (greater than 0.8) for slopes greater than 30° and soil thicknesses ranging from 3 to 1 m for slopes ranging from 30° to 60° respectively. While PoF_STV shows the same behavior for soil thicknesses ranging from 5 to 1 m (Figure 6c).

Figure 6d shows the difference between the mean PoF_STV and the mean PoF_ST as a function of slope and soil thickness. A general decrease of the probability is visible for slopes ranging from 17° to 60° and thicknesses between 0.5 and 10m (Figure 6d). However, the strongest decrease (more than -0.15) is observed for slopes ranging from 30° to 60° and soil thicknesses ranging from 1 to 3 m (Figure 6d). The presence of tall vegetation has a maximum impact (-0.39) for slopes of 48° and soil thickness of 1.25 m. It also has a major impact, reducing the mean probability by more than -0.3 for slopes angles and soil thickness ranging from 37 to 50° and 1.8 to 2.5 m, respectively.

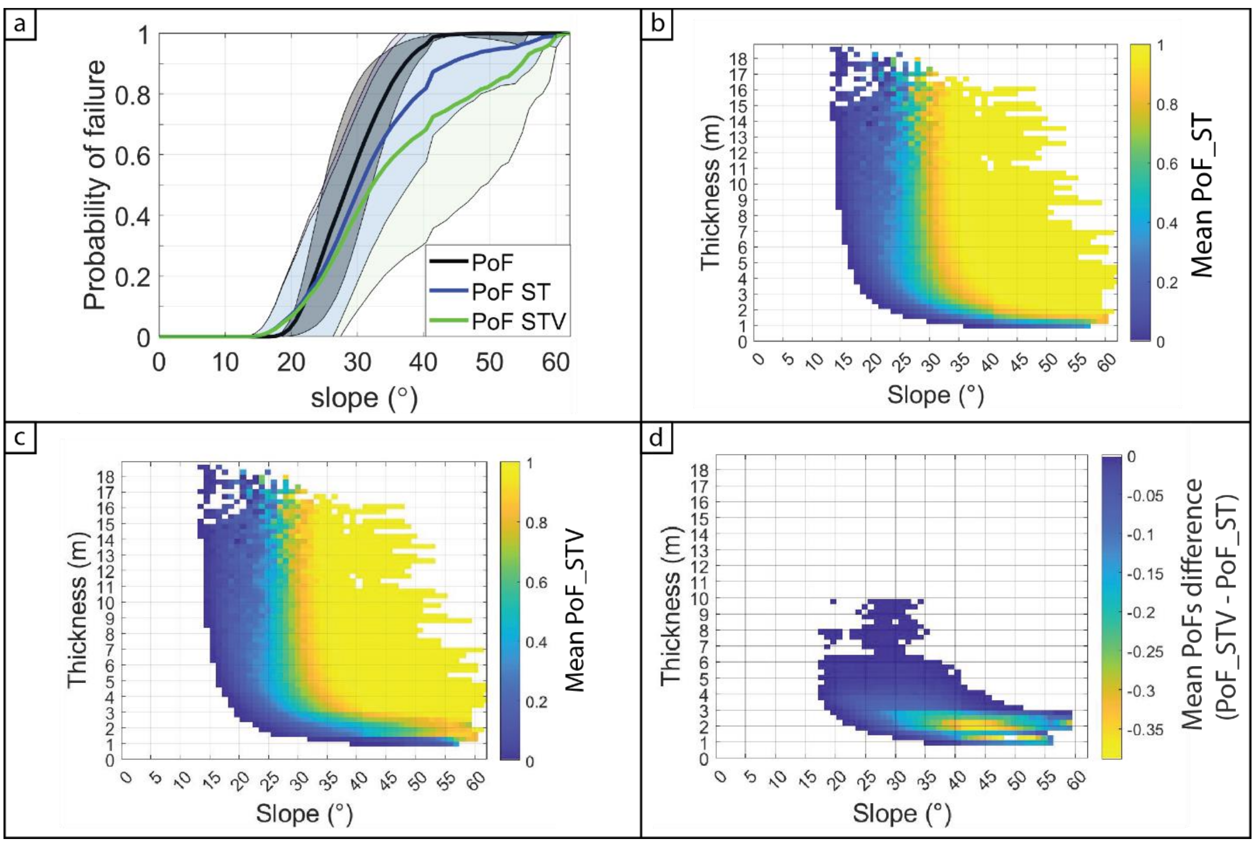

Figure 6 a) Mean PoF (black), PoF_ST (blue) and PoF_STV (green) as a function of slope angle and the associated variability across the site expressed as standard deviation b) Mean PoF_ST as a function of slope angle and soil *thickness c) Mean PoF_STV as a function of slope angle and soil thickness d) Difference of mean PoF_STV and mean PoF_ST as a function of slope angle and soil thickness.*

4.5. PoF monitoring

During the monitoring period, eucalyptus trees were harvested to reduce the risk of fire. This management was taken into account in the study in order to have an updated PoF. However, in order to emphasize the importance of monitoring the vegetation cover, we also assessed the PoF before the trees were removed.

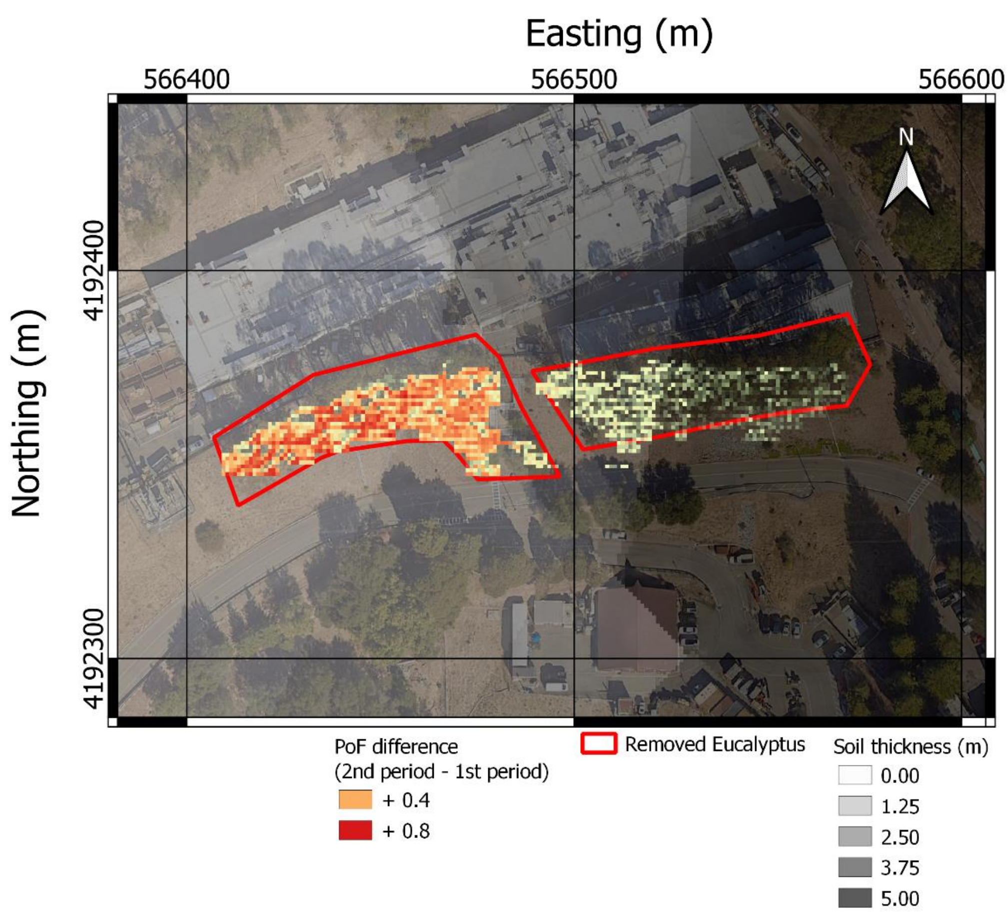

Figure 7: PoF difference between the second and the first period respectively after and before Eucalyptus removal. Red areas highlighted the managed area. Soil thickness is displayed in grey scale between 0 and 5 m.

Figure 7 shows the difference in the PoF after the removal of Eucalyptus (2^{nd} period – 1^{st} period). A considerable increase in the PoF is observed up to +0.8 due to the absence of Eucalyptus. The PoF increased more in the western part of the area due to thinner soil (less than 2.5 m, Figure 7). The eastern part, with a soil thickness of 5 m, is only slightly affected (+ 0.1).

5. Discussion

The PoF of a highly landslide-prone urban area was evaluated. We showed through a sensitivity analysis that for our study case the impactful parameters on the PoF calculation are the slope angle, the soil thickness, and the cohesion. The sensitivity analysis showed that the slope angle has the greatest influence. The soil thickness and cohesion are shown to have a similar influence on the PoF calculation. While the slope angle can be readily extracted from a high-resolution DEM, estimating the distribution of soil thickness and cohesion is more challenging. In order to retrieve spatial variations in soil thickness and root cohesion, we applied two methods that are not time-consuming and tedious from the perspective of easy reproducibility. The recording of ambient seismic noise gave easy access to soil thickness and the classification of satellite images allowed rapid and repeatable mapping of vegetation cover, directly related to the root network.
The computation of the PoF only considering slope angles showed that increasing slope angle from 20° to 50° drastically increases the PoF until reaching a plateau close to a PoF of 1.
Considering the variation in soil thickness reduced the global PoF over the area from 0.28. to 0.22. We showed that, for slopes above 30°, thicknesses above 5 m lead to a PoF of 0.9 and higher, highlighting a very high landslide hazard. In addition, the increased amount of potential sliding mass could result in devastating impacts of landslides in these areas. Figure 8a shows that, overall, consideration of the impact of soil thickness variations led to localized the high PoFs in areas of paleolandslides and active landslides. Rare exceptions can be seen in some built areas, where the probable excavation leading to the reduction of the soil thickness locally

mitigates the risk of landslides. On the contrary, the majority of locations without any history of sliding show a small PoFs when taking into account the soil thickness variations. The northwestern part of the study area, which does not present a history of landslides, shows a very high PoF due to the presence of steep slopes (>30°) and thick soils (>8 m). This demonstrates that it is very likely that a future slide event will occur in this area.

We globally evaluated the soil cohesion from previous geotechnical campaigns. We used a remote sensing approach to extract the vegetation cover and hence root cohesion. We showed that root cohesion has a significant impact on slope stabilization, particularly under thin soil conditions. Root cohesion has a beneficial impact, lowering the PoF drastically for soil thickness lower than 3 m with slope angles between 30 and 60°, with the larger impact for soil thickness of 2 m and below. This shows that the root network is not dense enough to have a significant benefit for deeper soil. In most of the cases, the root network will not reach depths larger than 7 m with a small fraction of them going deeper than 1 m (Canadell et al., 1996) and approximately 70% of root biomass located above 50 cm depth for woody species (Jackson et al., 1996; Kummerow and Mangan, 1981; Schulze et al., 1996). In case of larger soil thickness, vegetation could have a negative impact, adding weight to the soil, which would increase the PoF. However, we did not evaluate this impact because: (i) it was impossible to evaluate stem weight distribution from our method since we mapped the canopy, (ii) surcharge effect is often negligible compare to the soil mass itself (Fan and Lai, 2014), even more in case of relatively deep landslides. Figure 8b, showing the difference PoF with and without added root cohesion (respectively PoF_STV and PoF_ST), and demonstrates the impact of root cohesion on slope stabilization. It shows a reduction in PoF in areas without landslides history, but also in some paleolandslides areas. This highlighted the fact that some paleolandslides may have been mitigated by the natural or man-made addition of vegetation.

Finally, considering soil properties of the study area, we showed that a slope of 20° is required to trigger a landslide, with a higher probability for slopes of 30° and greater. Then, sufficient weight is required to reach the slope failure. To reach this threshold, a soil thickness of at least 1 m is required to trigger a landslide in steep slope areas (> 55°) and at least 3 m in gentler slope areas (about 20°).

Overall, the study showed that each parameter could have a significant effect on the final PoF assessment. Average annual displacement rates were recovered for five GPS stations using velocities calculated by Murray and Svarc (2017) from which the velocity of GNSS station P224 was subtracted to abrogate for tectonic plate movement. The final PoF map considering the three parameters discussed here shows that the monitored locations exhibit displacements and are located in areas of a high PoF (Figure 8c). Indeed, all five GPS stations showed displacements ranging from 4.8 to 15.1 mm/yr. LRA5, located in an area listed as a paleolandslide shows yearly displacement of 5 mm/yr corresponding to a very slow-moving landslide. This demonstrates that the landslide hazard is still present in this area, even though it is classified as a paleolandslide, and that this is probably also the case for the other unmitigated areas.

The study showed that the soil thickness variability and vegetation distribution are of critical importance to the landslide risk evaluation. In that case considering both distributions was necessary to assess the PoF and the risk associated with future slope failures.
This study showed that geophysical measurements, and more precisely the computation of the HV ratio is efficient to extract the soil thickness at local to regional scale without requiring time-consuming and cumbersome methods. We have also shown that the use of remote sensing to extract vegetation cover is an easy and efficient way to retrieve the spatial distribution and evolution of root cohesion for the purpose of the PoF monitoring. Indeed, in our case, land use management in the study area, located in the Bay Area, has led to a large number of Eucalyptus removals due to fire hazards. Studies already implement a real time evaluation of the landslide hazard based on a physical based model (Krøgli et al., 2018) however only considering

meteorological forecast. We showed that tree removal increased drastically the PoF in thin soil areas. However, as shown by Schmidt et al., 2001, the added root cohesion last for few years after harvesting, depending on the tree species. The root cohesion decay after harvesting was not consider in this study to show the impact of harvesting on the PoF in the future however it should be considered in a monitoring purpose. For this, classifying the vegetation cover 3-4 times per year would allow for variations in vegetation cover, and thus root cohesion, to be considered from a real-time hazard assessment perspective. This would also provide a feedback pathway to adapt land management plans to include landslide hazard concerns.

The approach used in this study allowed us to consider the spatial variability of the slope, the cohesion and the soil thickness. In addition, the sensitivity analysis showed that uncertainties in soil density, friction angle and transmissivity have a small impact on the final PoF map. However, uncertainties in slope angle and soil thickness could have a major impact on the final PoF map. The slope angle uncertainty depends on the DEM used. In our case, the DEM used has a slope angle accuracy of about ±5°. We showed that soil thickness variations have a major impact in the 0-5 m range related to uncertainties ranging from 0 to 1 m, respectively. The two accuracies (slope angle and soil thickness) can impact the final PoF map, however, they are small enough not to challenge the overall conclusions discussed above.

As Corominas et al. (2013) stated, it is critical, before assessing the landslide risk of an area, to properly calibrate the impacting parameters without which the assessment could either over- or underestimate the risk, thereby providing an unreliable estimate.

547
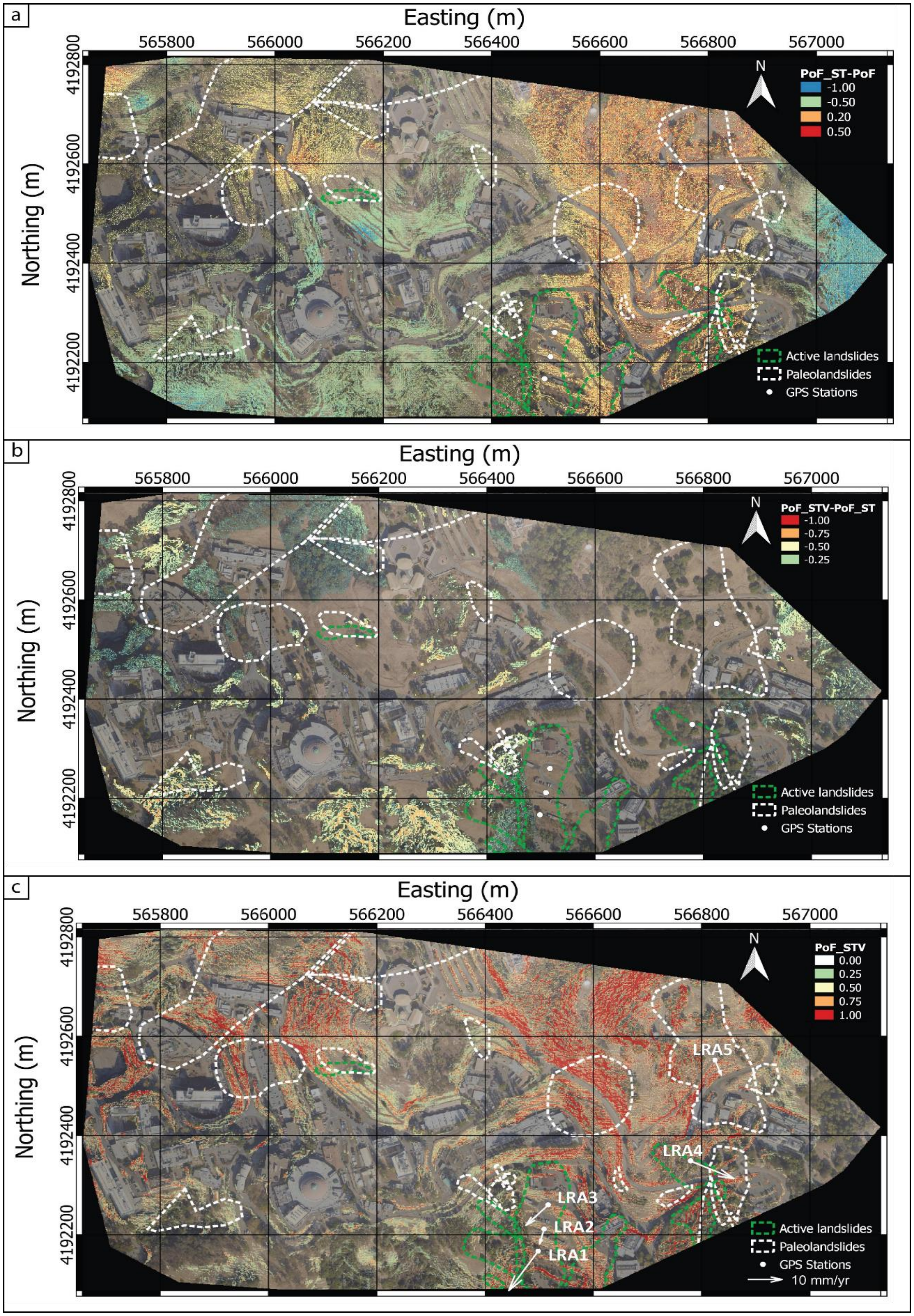
a
Easting (m)
565800
566000
566200
566400
566600
566800
567000
Northing (m)
4192800
4192600
4192400
4192200
N
PoF_ST-PoF
-1.00
-0.50
0.20
0.50
Active landslides
Paleolandslides
GPS Stations
b
Easting (m)
Northing (m)
PoF_STV-PoF_ST
-1.00
-0.75
-0.50
-0.25
Active landslides
Paleolandslides
GPS Stations
c
Easting (m)
Northing (m)
PoF_STV
0.00
0.25
0.50
0.75
1.00
LRA5
LRA4
LRA3
LRA2
LRA1
Active landslides
Paleolandslides
GPS Stations
10 mm/yr

Figure 8 Maps of active landslides and paleolandslides associated with a) the impact of soil thickness variation (PoF_ST – PoF), b) the impact of root cohesion (PoF_STV - PoF_ST) and c) PoF_STV and mean yearly displacement of GPS stations.

6. Conclusion/perspectives

This study shows that coupling geophysical and remote sensing data is useful to reduce uncertainty in the assessment of landslide hazards. We were able to evaluate the slope angle, the soil thickness, and root cohesion influence on slope stability. We highlighted that, for this study area, slope angles above 30° have a high PoF (>0.5). Additionally, we showed that the soil thickness variability has a strong impact on the PoF of the study area. Soil thicknesses greater than 5 m significantly increase the PoF for slope angles of 30° and greater. For thinner soil cover (1m - 5m), the PoF were generally low, but for very steep slopes, values of up to 1 are still possible, with higher possibility at smaller angles for increasing soil thickness (i.e. 35° for 5 m, and 55° for 2 m soil thickness). We were also able to show that root cohesion is only effective in slope stabilization for very shallow soil thicknesses (< 3 m). Our results demonstrate that the knowledge of the soil thickness distribution is essential to properly evaluate the PoF of a study area. While assuming a constant soil thickness across the area showed a high PoF throughout the study site, acknowledging variable thickness and vegetation distribution highlighted areas of an increased PoF. These areas characterized by a high PoF also correlate with areas of known and currently monitored slope displacements, but also highlighted other areas of concern.

In general, we showed that it is critical to properly estimate the PoF in such an urban area and to address the impact of critical parameters such as soil thickness and added cohesion. To help with that, we propose a new approach combining the use of ambient seismic noise and remote sensing data allowing to extract these parameters easily. The use of ambient noise shows that we can easily extract the soil thickness in short time. We show promising results for monitoring the PoF using remote sensing in such evolving areas. A second step would be to track changes in soil parameters to update the PoF over time. To do this, a network of sensors measuring the water table and soil moisture continuously would provide no longer an average PoF, but a close to real time PoF which could lead to early warning systems. Our study highlights the importance of a good understanding of the soil thickness and vegetation distribution for landslide hazard assessment, but also provides a novel and transferable methodology to account for those in the assessment.

Acknowledgments

We would like to thank the NASA Commercial Smallsat Data Acquisition (CSDA) program for providing access to the Planet data used in this study.

Funding

This research has been supported by a Laboratory Directed Research and Development Grant awarded to Sebastian Uhlemann.

A3GEO, Inc., 2020. Geotechnical Data and Interpretations Report Fiscal Year 2020 Ground Motions Study Lawrence Berkeley National Laboratory Berkeley, California.

Akgun, A., 2012. A comparison of landslide susceptibility maps produced by logistic regression, multi-criteria decision, and likelihood ratio methods: a case study at İzmir, Turkey. Landslides 9, 93–106. https://doi.org/10.1007/s10346-011-0283-7

Aleotti, P., Chowdhury, R., 1999. Landslide hazard assessment: summary review and new perspectives. Bull. Eng. Geol. Environ. 58, 21–44. https://doi.org/10.1007/s100640050066

An, H., Viet, T.T., Lee, G., Kim, Y., Kim, M., Noh, S., Noh, J., 2016. Development of time-variant landslide-prediction software considering three-dimensional subsurface unsaturated flow. Environ. Model. Softw. 85, 172–183. https://doi.org/10.1016/j.envsoft.2016.08.009

Anagnostopoulos, G.G., Fatichi, S., Burlando, P., 2015. An advanced process-based distributed model for the investigation of rainfall-induced landslides: The effect of process representation and boundary conditions. Water Resour. Res. 51, 7501–7523. https://doi.org/10.1002/2015WR016909

Band, L.E., Hwang, T., Hales, T.C., Vose, J., Ford, C., 2012. Ecosystem processes at the watershed scale: Mapping and modeling ecohydrological controls of landslides. Geomorphology, Geospatial Technologies and Geomorphological Mapping Proceedings of the 41st Annual Binghamton Geomorphology Symposium 137, 159–167. https://doi.org/10.1016/j.geomorph.2011.06.025

Baum, L., Savage, W.Z., Godt, J.W., 2008. TRIGRS-A Fortran program for transient rainfall infiltration and grid-based regional slope-stability analysis, version 2.0, US Geological Survey Open-File Report 2008–1159, available at: http://pubs.usgs. gov/of/2008/1159.

Canadell, J., Jackson, R.B., Ehleringer, J.B., Mooney, H.A., Sala, O.E., Schulze, E.-D., 1996. Maximum rooting depth of vegetation types at the global scale. Oecologia 108, 583–595. https://doi.org/10.1007/BF00329030

Cervi, F., Berti, M., Borgatti, L., Ronchetti, F., Manenti, F., Corsini, A., 2010. Comparing predictive capability of statistical and deterministic methods for landslide susceptibility mapping: a case study in the northern Apennines (Reggio Emilia Province, Italy). Landslides 7, 433–444. https://doi.org/10.1007/s10346-010-0207-y

Chen, T., Niu, R., Jia, X., 2016. A comparison of information value and logistic regression models in landslide susceptibility mapping by using GIS. Environ. Earth Sci. 75, 867. https://doi.org/10.1007/s12665-016-5317-y

Chen, W., Wang, J., Xie, X., Hong, H., Van Trung, N., Bui, D.T., Wang, G., Li, X., 2016. Spatial prediction of landslide susceptibility using integrated frequency ratio with entropy and support vector machines by different kernel functions. Environ. Earth Sci. 75, 1344. https://doi.org/10.1007/s12665-016-6162-8

Chen, W., Xie, X., Wang, J., Pradhan, B., Hong, H., Bui, D.T., Duan, Z., Ma, J., 2017. A comparative study of logistic model tree, random forest, and classification and regression tree models for spatial prediction of landslide susceptibility. CATENA 151, 147–160. https://doi.org/10.1016/j.catena.2016.11.032

Choo, H., Min, D.-H., Sung, J.H., Yoon, H.-K., 2019. Sensitivities of input parameters for predicting stability of soil slope. Bull. Eng. Geol. Environ. 78, 5671–5685. https://doi.org/10.1007/s10064-019-01503-4

Cohen, D., Schwarz, M., 2017. Tree-root control of shallow landslides. Earth Surf. Dyn. 5, 451–477. https://doi.org/10.5194/esurf-5-451-2017

Cohen-Waeber, J.F., 2018. Spatiotemporal Patterns of Seasonality in Landslide Deformation from InSAR and GPS (Ph.D.). University of California, Berkeley, United States -- California.

Corominas, J., van Westen, C., Frattini, P., Cascini, L., Malet, J.-P., Fotopoulou, S., Catani, F., Van Den Eeckhaut, M., Mavrouli, O., Agliardi, F., Pitilakis, K., Winter, M.G., Pastor, M., Ferlisi, S., Tofani, V., Hervás, J., Smith, J.T., 2013. Recommendations for the quantitative analysis of landslide risk. Bull. Eng. Geol. Environ. https://doi.org/10.1007/s10064-013-0538-8

Devkota, K.C., Regmi, A.D., Pourghasemi, H.R., Yoshida, K., Pradhan, B., Ryu, I.C., Dhital, M.R., Althuwaynee, O.F., 2013. Landslide susceptibility mapping using certainty factor, index of entropy and logistic regression models in GIS and their comparison at Mugling–Narayanghat road section in Nepal Himalaya. Nat. Hazards 65, 135–165. https://doi.org/10.1007/s11069-012-0347-6

Emadi-Tafti, M., Ataie-Ashtiani, B., Hosseini, S.M., 2021. Integrated impacts of vegetation and soil type on slope stability: A case study of Kheyrud Forest, Iran. Ecol. Model. 446, 109498. https://doi.org/10.1016/j.ecolmodel.2021.109498

Forbes, K., Broadhead, J., 2013. Forests and landslides: The role of trees and forests in the prevention of landslides and rehabilitation of landslide-affected areas in Asia. Food and Agriculture Organization of the United Nations, Bangkok.

Froude, M.J., Petley, D., 2018. Global Fatal Landslide Occurrence from 2004 to 2016. Nat. Hazards Earth Syst. Sci. 18, 2161–2181.

Gorsevski, P.V., Brown, M.K., Panter, K., Onasch, C.M., Simic, A., Snyder, J., 2016. Landslide detection and susceptibility mapping using LiDAR and an artificial neural network approach: a case study in the Cuyahoga Valley National Park, Ohio. Landslides 13, 467–484. https://doi.org/10.1007/s10346-015-0587-0

Guéguen, P., Cornou, C., Garambois, S., Banton, J., 2007. On the Limitation of the H/V Spectral Ratio Using Seismic Noise as an Exploration Tool: Application to the Grenoble Valley (France), a Small Apex Ratio Basin. Pure Appl. Geophys. 164, 115–134. https://doi.org/10.1007/s00024-006-0151-x

Guzzetti, F., Carrara, A., Cardinali, M., Reichenbach, P., 1999. Landslide Hazard Evaluation: A Review of Current Techniques and Their Application in a Multi-Scale Study, Central Italy. Geomorphology 31, 181–216. https://doi.org/10.1016/S0169-555X(99)00078-1

Hammond, C.J., Prellwitz, R.W., Miller, S.M., 1992. Landslide hazard assessment using Monte Carlo simulation, in: Proceedings of 6th International Symposium on Landslides, Christchurch, New Zealand, Balkema. pp. 251–294.

Hobley, D.E.J., Adams, J.M., Nudurupati, S.S., Hutton, E.W.H., Gasparini, N.M., Istanbulluoglu, E., Tucker, G.E., 2017. Creative computing with Landlab: an open-source toolkit for building, coupling, and exploring two-dimensional numerical models of Earth-surface dynamics. Earth Surf. Dyn. 5, 21–46. https://doi.org/10.5194/esurf-5-21-2017

Hungr, O., Leroueil, S., Picarelli, L., 2014. The Varnes classification of landslide types, an update. Landslides 11, 167–194. https://doi.org/10.1007/s10346-013-0436-y

Hwang, T., Band, L.E., Hales, T.C., Miniat, C.F., Vose, J.M., Bolstad, P.V., Miles, B., Price, K., 2015. Simulating vegetation controls on hurricane-induced shallow landslides with a distributed ecohydrological model. J. Geophys. Res. Biogeosciences 120, 361–378. https://doi.org/10.1002/2014JG002824

Ji, J., Kokutse, N., Genet, M., Fourcaud, T., Zhang, Z., 2012. Effect of spatial variation of tree root characteristics on slope stability. A case study on Black Locust (Robinia pseudoacacia) and Arborvitae (Platycladus orientalis) stands on the Loess Plateau, China. CATENA 92, 139–154. https://doi.org/10.1016/j.catena.2011.12.008

Jones, D.L., Curtis, G.H., 1991. Guide to the geology of the Berkeley Hills, central Coast Ranges, California. Geol. Excursions North. Calif. San Franc. Sierra Nev. Calif. Div. Mines Geol. Spec. Publ. 109, 63–74.

Jovančević, S.D., Nagai, O., Sassa, K., Arbanas, Ž., 2013. Deterministic Landslide Susceptibility Analyses Using LS-Rapid Software 5.

Kalantar, B., Ueda, N., Saeidi, V., Ahmadi, K., Halin, A.A., Shabani, F., 2020. Landslide Susceptibility Mapping: Machine and Ensemble Learning Based on Remote Sensing Big Data. Remote Sens. 12, 1737. https://doi.org/10.3390/rs12111737

Kim, J.H., Fourcaud, T., Jourdan, C., Maeght, J.-L., Mao, Z., Metayer, J., Meylan, L., Pierret, A., Rapidel, B., Roupsard, O., de Rouw, A., Sanchez, M.V., Wang, Y., Stokes, A., 2017. Vegetation as a driver of temporal variations in slope stability: The impact of hydrological processes. Geophys. Res. Lett. 44, 4897–4907. https://doi.org/10.1002/2017GL073174

Konno, K., Ohmachi, T., 1998. Ground-motion characteristics estimated from spectral ratio between horizontal and vertical components of microtremor. Bull. Seismol. Soc. Am. 88, 228–241. https://doi.org/10.1785/BSSA0880010228

Kramer, S.L., 1996. Earthquake Geotechnical Engineering. Prentice Hall, Upper Saddle River, NJ.

Kropp Alan, Associates, 2006. Initial landslide characterization study East Canyon–Buildings 85 and 85A.

Kuriakose, S.L., van Beek, L.P.H., 2011. Plant Root Strength and Slope Stability, in: Gliński, J., Horabik, J., Lipiec, J. (Eds.), Encyclopedia of Agrophysics. Springer Netherlands, Dordrecht, pp. 622–627. https://doi.org/10.1007/978-90-481-3585-1_222

Le Roux, O., Schwartz, S., Gamond, J.F., Jongmans, D., Tricart, P., Sebrier, M., 2010. Interaction between tectonic and erosion processes on the morphogenesis of an Alpine valley: geological and geophysical investigations in the lower Romanche valley (Belledonne massif, western Alps). Int. J. Earth Sci. 99, 427–441. https://doi.org/10.1007/s00531-008-0393-1

Lee, S., Jang, J., Kim, Y., Cho, N., Lee, M.-J., 2020. Susceptibility Analysis of the Mt. Umyeon Landslide Area Using a Physical Slope Model and Probabilistic Method. Remote Sens. 12, 2663. https://doi.org/10.3390/rs12162663

Li, S.H., Luo, X.H., Wu, L.Z., 2021. A new method for calculating failure probability of landslide based on ANN and a convex set model. Landslides 18, 2855–2867. https://doi.org/10.1007/s10346-021-01652-2

Marelli, S., Sudret, B., 2014. UQLab: A Framework for Uncertainty Quantification in Matlab 2554–2563. https://doi.org/10.1061/9780784413609.257

Marjanović, M., Kovačević, M., Bajat, B., Voženílek, V., 2011. Landslide susceptibility assessment using SVM machine learning algorithm. Eng. Geol. 123, 225–234. https://doi.org/10.1016/j.enggeo.2011.09.006

Mattia, C., Bischetti, G.B., Gentile, F., 2005. Biotechnical Characteristics of Root Systems of Typical Mediterranean Species. Plant Soil 278, 23–32. https://doi.org/10.1007/s11104-005-7930-5

Mergili, M., Marchesini, I., Rossi, M., Guzzetti, F., Fellin, W., 2014. Spatially distributed three-dimensional slope stability modelling in a raster GIS. Geomorphology 206, 178–195. https://doi.org/10.1016/j.geomorph.2013.10.008

Min, D.-H., Yoon, H.-K., 2021. Suggestion for a new deterministic model coupled with machine learning techniques for landslide susceptibility mapping. Sci. Rep. 11, 6594. https://doi.org/10.1038/s41598-021-86137-x

Montgomery, D.R., Dietrich, W.E., 1994. A physically based model for the topographic control on shallow landsliding. Water Resour. Res. 30, 1153–1171. https://doi.org/10.1029/93WR02979

Montoya-Araque, E.A., Suarez-Burgoa, L.O., 2018. pyBIMstab: Application software for 2D slope stability analysis of block-in-matrix and homogeneous materials. SoftwareX 7, 383–387. https://doi.org/10.1016/j.softx.2018.11.003

Montrasio, L., Valentino, R., Losi, G.L., 2011. Towards a real-time susceptibility assessment of rainfall-induced shallow landslides on a regional scale. Nat. Hazards Earth Syst. Sci. 11, 1927–1947. https://doi.org/10.5194/nhess-11-1927-2011

Mountrakis, G., Im, J., Ogole, C., 2011. Support vector machines in remote sensing: A review. ISPRS J. Photogramm. Remote Sens. 66, 247–259. https://doi.org/10.1016/j.isprsjprs.2010.11.001

Murray, J.R., Svarc, J., 2017. Global Positioning System Data Collection, Processing, and Analysis Conducted by the U.S. Geological Survey Earthquake Hazards Program. Seismol. Res. Lett. 88, 916–925. https://doi.org/10.1785/0220160204

Nilsen, B., 2000. New trends in rock slope stability analyses. Bull. Eng. Geol. Environ. 58, 173–178. https://doi.org/10.1007/s100640050072

Nourani, V., Pradhan, B., Ghaffari, H., Sharifi, S.S., 2014. Landslide susceptibility mapping at Zonouz Plain, Iran using genetic programming and comparison with frequency ratio, logistic regression, and artificial neural network models. Nat. Hazards 71, 523–547. https://doi.org/10.1007/s11069-013-0932-3

Pack, R.T., Tarboton, D.G., Goodwin, C.N., 1999. SINMAP 2.0-A stability index approach to terrain stability hazard mapping, user's manual.

Palazzolo, N., Peres, D.J., Bordoni, M., Meisina, C., Creaco, E., Cancelliere, A., 2021. Improving Spatial Landslide Prediction with 3D Slope Stability Analysis and Genetic Algorithm Optimization: Application to the Oltrepò Pavese. Water 13, 801. https://doi.org/10.3390/w13060801

Park, S., Choi, C., Kim, B., Kim, J., 2013. Landslide susceptibility mapping using frequency ratio, analytic hierarchy process, logistic regression, and artificial neural network methods at the Inje area, Korea. Environ. Earth Sci. 68, 1443–1464. https://doi.org/10.1007/s12665-012-1842-5

Pedregosa, F., Varoquaux, G., Gramfort, A., Michel, V., Thirion, B., Grisel, O., Blondel, M., Prettenhofer, P., Weiss, R., Dubourg, V., Vanderplas, J., Passos, A., Cournapeau, D., Brucher, M., Perrot, M., Duchesnay, É., 2011. Scikit-learn: Machine Learning in Python. J. Mach. Learn. Res. 12, 2825–2830.

Phillips, C., Hales, T., Smith, H., Basher, L., 2021. Shallow landslides and vegetation at the catchment scale: A perspective. Ecol. Eng. 173, 106436. https://doi.org/10.1016/j.ecoleng.2021.106436

Preti, F., 2006. On root reinforcement modeling. European Geosciences Union 2006, in: Geophysical Research Abstracts. p. 04555.

Probabilities (WGCEP), W.G. on C.E., 2008. The uniform California earthquake rupture forecast, version 2 (UCERF 2). US Geol. Surv. Open File Rep. 2007-1437 Calif. Geol. Surv. Spec. Rep. 203.

Quantum Spatial, I., 2019. Northern California 3DEP QL1 QL2 LiDAR Project Report.

Regmi, A.D., Devkota, K.C., Yoshida, K., Pradhan, B., Pourghasemi, H.R., Kumamoto, T., Akgun, A., 2014. Application of frequency ratio, statistical index, and weights-of-evidence models and their comparison in landslide susceptibility mapping in Central Nepal Himalaya. Arab. J. Geosci. 7, 725–742. https://doi.org/10.1007/s12517-012-0807-z

Reichenbach, P., Rossi, M., Malamud, B.D., Mihir, M., Guzzetti, F., 2018. A review of statistically-based landslide susceptibility models. Earth-Sci. Rev. 180, 60–91. https://doi.org/10.1016/j.earscirev.2018.03.001

Reid, M.E., Christian, S.B., Brien, D.L., Henderson, S.T., 2015. Scoops3D: software to analyze 3D slope stability throughout a digital landscape (USGS Numbered Series No. 14-A1), Scoops3D: software to analyze 3D slope stability throughout a digital landscape, Techniques and Methods. U.S. Geological Survey, Reston, VA. https://doi.org/10.3133/tm14A1

Rossi, G., Catani, F., Leoni, L., Segoni, S., Tofani, V., 2013. HIRESSS: a physically based slope stability simulator for HPC applications. Nat. Hazards Earth Syst. Sci. 13, 151–166. https://doi.org/10.5194/nhess-13-151-2013

Segoni, S., Rossi, G., Catani, F., 2012. Improving basin scale shallow landslide modelling using reliable soil thickness maps. Nat. Hazards 61, 85–101. https://doi.org/10.1007/s11069-011-9770-3

SESAME, 2004. Guidelines for the Implementation of the H/V Spectral Ratio Technique on Ambient Vibrations: Measurements, Processing and Interpretation, SESAME European Research Project, WP12—Deliverable D23, 12. EVG1-CT-2000-00026, 1– 62.

Sidle, R.C., Bogaard, T.A., 2016. Dynamic earth system and ecological controls of rainfall-initiated landslides. Earth-Sci. Rev. 159, 275–291. https://doi.org/10.1016/j.earscirev.2016.05.013

Sidle, R.C., Ochiai, H., 2006. Landslides: Processes, Prediction and Land Use, Water Resources Monograph. American Geophysical Union, Washington, DC.

Simoni, S., Zanotti, F., Bertoldi, G., Rigon, R., 2008. Modelling the probability of occurrence of shallow landslides and channelized debris flows using GEOtop-FS. Hydrol. Process. 22, 532–545. https://doi.org/10.1002/hyp.6886

Sobol′, I.M., 2001. Global sensitivity indices for nonlinear mathematical models and their Monte Carlo estimates. Math. Comput. Simul., The Second IMACS Seminar on Monte Carlo Methods 55, 271–280. https://doi.org/10.1016/S0378-4754(00)00270-6

Strauch, R., Istanbulluoglu, E., Nudurupati, S.S., Bandaragoda, C., Gasparini, N.M., Tucker, G.E., 2018. A hydroclimatological approach to predicting regional landslide probability using Landlab. Earth Surf. Dyn. 6, 49–75. https://doi.org/10.5194/esurf-6-49-2018

Sudmeyer, R.A., Speijers, J., Nicholas, B.D., 2004. Root distribution of Pinus pinaster, P. radiata , Eucalyptus globulus and E. kochii and associated soil chemistry in agricultural land adjacent to tree lines †. Tree Physiol. 24, 1333–1346. https://doi.org/10.1093/treephys/24.12.1333

Thiebes, B., Bell, R., Glade, T., Jäger, S., Anderson, M., Holcombe, L., 2013. A WebGIS decision-support system for slope stability based on limit-equilibrium modelling. Eng. Geol. 158, 109–118. https://doi.org/10.1016/j.enggeo.2013.03.004

Tien Bui, D., Tuan, T.A., Klempe, H., Pradhan, B., Revhaug, I., 2016. Spatial prediction models for shallow landslide hazards: a comparative assessment of the efficacy of support vector machines, artificial neural networks, kernel logistic regression, and logistic model tree. Landslides 13, 361–378. https://doi.org/10.1007/s10346-015-0557-6

Tsangaratos, P., Benardos, A., 2014. Estimating landslide susceptibility through a artificial neural network classifier. Nat. Hazards 74, 1489–1516. https://doi.org/10.1007/s11069-014-1245-x

Uhlemann, S., Chambers, J., Meldrum, P., McClure, P., Dafflon, B., 2021. Geophysical Monitoring of Landslides–A Step Closer Towards Predictive Understanding?, in: Casagli, N., Tofani, V., Sassa, K., Bobrowsky, P.T., Takara, K. (Eds.), Understanding and Reducing Landslide Disaster Risk: Volume 3 Monitoring and Early Warning, ICL Contribution to Landslide Disaster Risk Reduction. Springer International Publishing, Cham, pp. 85–91. https://doi.org/10.1007/978-3-030-60311-3_8

van Westen, C.J., van Asch, T.W.J., Soeters, R., 2006. Landslide hazard and risk zonation—why is it still so difficult? Bull. Eng. Geol. Environ. 65, 167–184. https://doi.org/10.1007/s10064-005-0023-0

Vandromme, R., Thiery, Y., Bernardie, S., Sedan, O., 2020. ALICE (Assessment of Landslides Induced by Climatic Events): A single tool to integrate shallow and deep landslides for susceptibility and hazard assessment. Geomorphology 367, 107307. https://doi.org/10.1016/j.geomorph.2020.107307

Wahrhaftig, C., Sloan, D., 1989. Geology of San Francisco and vicinity. Am. Geophys. Union.

Waldron, L.J., 1977. The Shear Resistance of Root-Permeated Homogeneous and Stratified Soil. Soil Sci. Soc. Am. J. 41, 843–849. https://doi.org/10.2136/sssaj1977.03615995004100050005x

Wathelet, M., Jongmans, D., Ohrnberger, M., 2004. Surface-wave inversion using a direct search algorithm and its application to ambient vibration measurements. Surf. Geophys. 2, 211–221. https://doi.org/10.3997/1873-0604.2004018

Wu, T.H., McKinnell III, W.P., Swanston, D.N., 1979. Strength of tree roots and landslides on Prince of Wales Island, Alaska. Can. Geotech. J. 16, 19–33. https://doi.org/10.1139/t79-003

Yilmaz, I., 2010a. The effect of the sampling strategies on the landslide susceptibility mapping by conditional probability and artificial neural networks. Environ. Earth Sci. 60, 505–519. https://doi.org/10.1007/s12665-009-0191-5

Yilmaz, I., 2010b. Comparison of landslide susceptibility mapping methodologies for Koyulhisar, Turkey: conditional probability, logistic regression, artificial neural networks, and support vector machine. Environ. Earth Sci. 61, 821–836. https://doi.org/10.1007/s12665-009-0394-9

Youssef, A.M., Pourghasemi, H.R., Pourtaghi, Z.S., Al-Katheeri, M.M., 2016. Landslide susceptibility mapping using random forest, boosted regression tree, classification and regression tree, and general linear models and comparison of their performance at Wadi Tayyah Basin, Asir Region, Saudi Arabia. Landslides 13, 839–856. https://doi.org/10.1007/s10346-015-0614-1

Zizioli, D., Meisina, C., Valentino, R., Montrasio, L., 2013. Comparison between different approaches to modeling shallow landslide susceptibility: a case history in Oltrepo Pavese, Northern Italy. Nat. Hazards Earth Syst. Sci. 13, 559–573. https://doi.org/10.5194/nhess-13-559-2013